Appl. Phys. B 87, 417–423 (2007)
DOI: 10.1007/s00340-007-2614-x

Applied Physics B
Lasers and Optics

E.A. BARBOSA[1,✉]
J.F. CARVALHO[2]

Surface analysis by two-diode laser photorefractive holography

[1] Laboratório de Óptica Aplicada, Faculdade de Tecnologia de São Paulo, Pça Cel Fernando Prestes 30, 01124-060 São Paulo, Brazil
[2] Instituto de Física, Universidade Federal de Goiás, Caixa Postal 131, 94001-970 Goiânia, Brazil

Received: 30 November 2006 /
Revised version: 29 January 2007
Published online: 24 March 2007 •

ABSTRACT Shape measurement through holography using two diode lasers emitting in the red region and a sillenite $Bi_{12}TiO_{20}$ photorefractive crystal as a holographic medium is theoretically and experimentally studied. By properly aligning and tuning both lasers, a synthetic wavelength is obtained providing the contour fringes on the holographic image in single-exposure recordings. The influence of alignment and tuning of the lasers on the contour interval as well as the dependence of the interferogram visibility on the deviations from the Bragg regime was analysed. Contour intervals down to 150 μm where achieved and measurements of low-curvature and low-derivative surfaces were performed.

PACS 42.40.Ht; 42.40.Kw; 42.40.Pa

1 Introduction

Optical methods for surface shaping are powerful tools for non-destructive testing including material analysis, deformation and strain measurement, vibration analysis and industry applications like machine vision and enhancement of manufacturing processes. These noncontacting methods present high precision, accuracy and reproducibility. Interferometric techniques like electronic speckle pattern interferometry (ESPI) and holographic interferometry have the additional advantage of whole-field quantitative and qualitative analysis. Their general principle is to generate interference fringes corresponding to the contour lines of the studied surface, typically in two-exposure processes. This can be carried out through two-color interferometry with tunable lasers [1], tilting of the illuminating mirror [2], or optical setups with two illuminating beams [3]. Although such double exposure procedures are widely used in the fields of holographic and speckle profilometry, they can lead to errors due to the relatively long acquisition times for interferograms because interferometers have stringent stability requirements.

In order to overcome this drawback, multimode large free-spectral range (FSR) diode lasers have been successfully used as light sources in optical profilometry through multi–wavelength holographic recording in photorefractive crystals [4, 5]. This method provides single-exposure contour interferograms due to the multi-wavelength character of such lasers [6]. The resultant diffraction efficiency depends on the difference between the optical paths of the reference and the object waves, and the resulting holographic image is spatially modulated by interference contour fringes. These fringes are the region of intersection of the object wavefront with planes of constant elevation which, in turn, are perpendicular to the bisector of the illuminating and scattered beams. It has been shown elsewhere [6] that the contour interval Δz (i.e., the distance between two consecutive planes) equals the laser resonator length L when the illuminating and the scattered beams propagate in opposite directions. For this reason the short-cavity diode lasers are the most suitable light sources for holographic profilometry purposes when the studied surface presents depth differences of the order of a few millimeters.

The ability to obtain single-exposure interferograms represents an obvious advantage of multi-wavelength holographic profilometry over other techniques which require two-exposure processes for fringe pattern generation: by using multimode diode lasers additional procedures like laser tuning or mirror tilting are not necessary, so that contour fringes can be obtained in real-time, single-exposure processes. This leads to faster and more accurate measurements and the whole experimental setup can be simpler and more compact than those used in two-exposure holographic techniques. This advantage exists regardless of the method used for fringe evaluation, such as phase- stepping or Fourier transform techniques.

One drawback to this method is that the contour interval cannot be changed because the length of the diode laser is constant. Remarkably, this limits the technique in the measurement of nearly flat surfaces or regions with low-derivative reliefs, which require smaller Δz values in order to minimize the measurement noise. Some alternatives have been presented in the literature in order to overcome this limitation: a holographic setup with two properly-shifted reference beams [4], the positioning of a Fabry–Pérot etalon at the laser output in order to increase the effective laser free spectral range [7] and the use of an eight-stepping procedure for interferogram evaluation through multi-wavelength electronic speckle pattern interferometry (ESPI) [8]. The free spectral range $\Delta\nu$ of the diode laser used in these studies is 53 GHz, corresponding to a wavelength gap $\Delta\lambda$ between consecutive modes

✉ Fax: +55 11 3315 8498, E-mail: ebarbosa@fatecsp.br

of 0.082 nm, a synthetic wavelength $\lambda^2/\Delta\lambda = 5.30$ mm and a contour interval $\Delta z \cong \lambda^2/2\Delta\lambda = 2.65$ mm. Among these studies, the smallest contour interval was obtained by employing a Fabry–Pérot etalon in order to re-inject some specific frequencies back into the diode laser. Thus, larger values of the emission free spectral range were achieved, providing contour intervals down to 0.88 mm and enabling less noisy and more accurate measurements.

In order to obtain smaller values of Δz and improve the measurement sensitivity, this work proposes an optical setup for real-time holographic profilometry with sillenite $Bi_{12}TiO_{20}$ (BTO) crystals employing two diode lasers emitting in the red region. The central wavelengths of both lasers are tuned to allow the simultaneous illumination of the object with two slightly different wavelengths and providing a very wide range of Δz values. Other works reported analogous experiments performing surface contouring through ESPI, generating contour intervals of few millimeters [9, 10]. For holographic recording with thick BTO crystals, the achievement of small values of Δz is limited by the Bragg condition, since the diffraction efficiency drops significantly in the out-of-Bragg holographic reconstruction. This drawback is partially compensated by the fact that photorefractive holography is able to provide the best visibility and lowest noise interferograms compared to most whole-field interferometric techniques, thereby providing more accurate and reproducible results. In the present work, the dependence of the diffraction efficiency and the interferogram visibility on the synthetic wavelength is experimentally investigated, as well as the influence of beam misalignment on the contour interval. In addition, alternatives for eliminating the low spatial frequency envelope generated in the holographic recording by each one of the multimode diode lasers are proposed. In the quantitative analysis, the fringe pattern was evaluated through the phase stepping technique (PST) [11] and the phase unwrapping was carried out by the Branch-cut method [12, 13].

2 Theoretical analysis

2.1 *Holographic recording and readout*

Let us consider the incidence of a reference and an object beam with amplitudes R_N and S_N, respectively, upon a photorefractive BTO crystal in a two-wave mixing scheme. Each beam originates from two properly aligned multimode diode lasers 1 and 2, and both lasers emit simultaneously N longitudinal modes with the same free spectral range (FSR) $\Delta\nu = c\Delta\lambda/\lambda^2$, with $\Delta\lambda$ being the wavelength gap between adjacent modes and c the light velocity. The emission of lasers 1 and 2 are centered at $k_1 \equiv 2\pi/\lambda_1$ and $k_2 \equiv 2\pi/\lambda_2$, respectively, where λ_1 and λ_2 are their respective central wavelengths. Thus, R_N and S_N can be written at the crystal input as

$$R_N = R_0\left(\mathrm{e}^{\mathrm{i}k_1\Gamma_R} + \mathrm{e}^{\mathrm{i}k_2\Gamma_R}\right)\sum_{n=-\frac{N-1}{2}}^{n=\frac{N-1}{2}} A_n \mathrm{e}^{\mathrm{i}(n\Delta k\Gamma_R+\varphi_n)}\,,$$

$$S_N = S_0\left(\mathrm{e}^{\mathrm{i}k_1\Gamma_S} + \mathrm{e}^{\mathrm{i}k_2\Gamma_S}\right)\sum_{n=-\frac{N-1}{2}}^{n=\frac{N-1}{2}} A_n \mathrm{e}^{\mathrm{i}(n\Delta k\Gamma_S+\varphi_n)}\,, \qquad (1)$$

where Γ_S and Γ_R are the optical paths of the object and the reference beams, respectively, $\Delta k = 2\pi\Delta\lambda/\lambda^2$, A_n is a real coefficient related to the n-th mode intensity and φ_n is the phase of the n-th mode at the laser output. The resulting interference pattern rearranges the charge carriers inside the crystal, giving rise to a spatially modulated electric field. Through the electrooptic effect this field generates a corresponding refractive index modulation forming a phase volume grating. The diffraction efficiency η of the recorded grating can be written as a function of the modulation index m of the interference pattern according to [14]

$$\eta \propto |m|^2 = \left|2\frac{R_N^* S_N}{|R_N|^2 + |S_N|^2}\right|^2\,, \qquad (2)$$

where * denotes complex conjugation. In the product $R_N^* S_N$ it shall be taken into account that two terms related to different wavelength numbers cannot be multiplied, since different modes are not mutually coherent [6]. For the same reason the phase difference $\varphi_n - \varphi_{n'}$ has a random temporal behavior if $n \neq n'$. Hence, from (1) and (2) the diffraction efficiency is given by

$$\eta \propto \left(\frac{2R_0S_0}{I_0}\right)^2 \cos^2\left[\frac{\pi}{\Lambda_S}(\Gamma_S - \Gamma_R)\right] \times \left|\sum_{n=-\frac{N-1}{2}}^{n=\frac{N-1}{2}} A_n \mathrm{e}^{\mathrm{i}n\Delta k(\Gamma_S-\Gamma_R)}\right|^2 \qquad (3)$$

where $I_0 = R_0^2 + S_0^2$ and $\Lambda_S \equiv \lambda_1\lambda_2/|\lambda_2 - \lambda_1|$ is the synthetic wavelength. For the sake of simplicity we assume that all modes in both lasers oscillate with the same intensity, so that $A_n = 1$. Thus, the diffraction efficiency becomes

$$\eta \propto \frac{2R_0S_0}{I_0}\cos^2\varphi\left[\frac{\sin(N\gamma)}{\sin(\gamma)}\right]^2\,, \qquad (4)$$

where $\varphi \equiv \pi(\Gamma_S - \Gamma_R)/\Lambda_S$ and $\gamma \equiv \Delta k(\Gamma_S - \Gamma_R)/2$. The holographic reconstruction in two-wave mixing occurs by self-diffraction, i.e. the reference beam is the readout beam. The holographic reconstruction I_S of the object is then given by

$$I_S = \eta I_R = \eta_0\cos^2\varphi\left[\frac{\sin(N\gamma)}{\sin(\gamma)}\right]^2 I_R\,, \qquad (5)$$

where I_R is the reference beam intensity and η_0 is the spatially unmodulated diffraction efficiency.

Equation (4) shows that the reconstructed object image appears to be doubly modulated by interference contour fringes. By tuning the diode lasers to get $|\lambda_2 - \lambda_1| \gg \Delta\lambda$, the resulting reconstructed image appears covered by high spatial frequency $\cos^2\varphi$-fringes generated by the lasers detuning. This in turn appears enveloped by a low spatial frequency $[\sin(N\gamma)/\sin\gamma]^2$-term which is due to the multi-wavelength emission of each diode laser. The intensity I_S is shown in Fig. 1 as a function of $\Delta\Gamma$ for $|\lambda_2 - \lambda_1| \cong 10$, $\Delta\lambda = 0.8$ nm and $N = 3$ modes according to (4).

The preceding analysis is valid provided the whole holographic reconstruction process occurs in the Bragg regime.

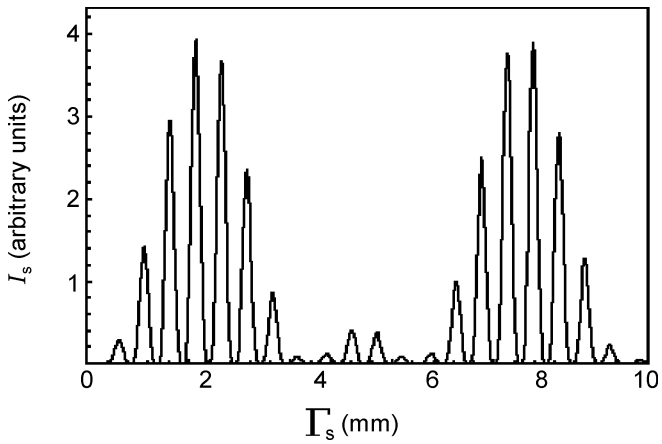

FIGURE 1 Intensity of the diffracted beam as a function of Γ_S for $|\lambda_2 - \lambda_1| \cong 10\Delta\lambda$ and $N = 3$

However, a more complete description of the involved phenomena must take into account eventual deviations from the Bragg conditions in order to evaluate the resulting interferogram visibility. Such deviations arise mainly from the lasers detuning, $\lambda_2 - \lambda_1$ and from eventual angular misalignments of the laser beams. If there are two wavelengths, two holographic gratings are recorded in the BTO crystal. In the readout process each wavelength, which produces small diffraction efficiencies, generates two mutually coherent diffracted waves with amplitudes proportional to $\sqrt{\eta_0}$ (self-diffraction, perfect Bragg regime) and $\chi\sqrt{\eta_0}$, where $\chi \equiv \sin\xi/\xi$. The phase ξ is given by $\xi = \frac{\vartheta d}{2\cos\theta}$, where d is the interaction length of the interfering beams inside the holographic medium, 2θ is the angle between the interfering beams and $\vartheta = \pi\left(\frac{2\Delta\alpha}{\lambda} - \frac{\lambda_2-\lambda_1}{n_0\lambda_2\lambda_1}\right)$ in our case is the dephasing measure introduced by Kogelnik in the coupled-wave theory for thick gratings [15]. The term $\Delta\alpha$ is the angular misalignment of the laser beams (which is also the deviation from the Bragg condition) and n_0 is the bulk refractive index of the medium. As the deviation from the Bragg condition increases, ϑ also increases but χ decreases. Thus, (5) can be written in a more rigorous form as

$$I_S = \eta_0\left(1 + \chi^2 + 2|\chi|\cos 2\varphi\right)\left[\frac{\sin(N\gamma)}{\sin(\gamma)}\right]^2 I_R\,. \tag{6}$$

From (6) the interferogram visibility V defined as $V = (I_{S\max} - I_{S\min}) / (I_{S\max} + I_{S\min})$ assumes the form

$$V = \frac{2|\chi|}{\chi^2 + 1}\,. \tag{7}$$

2.2 *Interferogram evaluation*

We employed the standard four-frame phase stepping technique (PST) for fringe pattern evaluation. This technique consists in sequentially acquiring and storing four $\pi/2$-phase-shifted interferograms with intensities I_{S0}, I_{S1}, I_{S2} and I_{S3}. A more detailed description of this procedure can be found elsewhere [4, 5]. The phase φ_S at a point (x, y) of the studied surface is given by the well-known formula [16]

$$\varphi_S(x, y) = \frac{1}{2}\arctan\left(\frac{I_{S1}(x, y) - I_{S3}(x, y)}{I_{S0}(x, y) - I_{S2}(x, y)}\right)\,, \tag{8}$$

where $I_{Si}(x, y)$ is the intensity at (x, y) for the ith-frame. It should be noticed, however, that (7) is not immediately applicable to the fringe pattern given by (5) or (6). The $[\sin(N\gamma)/\sin\gamma]^2$-term can be used in some specific cases for PST through holographic recording with only one multimode laser. In the present study, however, this term only modulates the $\cos^2\varphi$- pattern, which is the real object of interest. Two procedures can be adopted in order to eliminate the undesired influence of the envelope function: placement of a Fabry–Pérot etalon at the output of each laser, or proper positioning of the envelope maximum and decreasing the synthetic wavelength such that $\Lambda_S \ll \lambda^2/\Delta\lambda$. In the first case, the etalon reinjects some specific laser modes back into the laser resonator, enhancing the oscillation of these modes while suppressing the other modes [7]. This increases the effective free spectral range of the emission. If the gap t between the plane mirrors of the etalon is smaller than the laser resonator length L, only one mode can be selected from each laser, thus eliminating the $[\sin(N\gamma)/\sin\gamma]^2$-term. The other approach requires the acquisition of an interferogram when the entire studied surface is illuminated by a single low-frequency $[\sin(N\gamma)/\sin\gamma]^2$-fringe using one multimode laser, it shows the holographic image of a flat plate in Fig. 2a for $\lambda^2/\Delta\lambda = 5.30$ mm. The intensity profile of a cross section of the object is shown in the lower part of Fig. 2a. The contour interferogram of the same surface with two multimode lasers is shown in Fig. 2b for $\Lambda_S = 0.30$ mm, showing the respective intensity profile. By digitally dividing the image of Fig. 2b by that of Fig. 2a pixel-by-pixel, one obtains a non-modulated $\cos^2\varphi$-interferogram, as shown in Fig. 2c. This approach is limited to the analysis of surfaces with slight curvatures or with low derivative surfaces, which is the aim of our work.

2.3 *Contour interval considering laser misalignment*

The design of our optical setup was based upon two perfectly aligned and parallel laser beams. It is worthwhile, however, to evaluate the influence of an eventual angular misalignment of both beams on the contour interval Δz and show how this misalignment can be useful in enhancing the measurement sensitivity. Consider the incidence of the illuminating beams 1 and 2 on the object at angles α and $\alpha + \Delta\alpha$, respectively, as shown in Fig. 3.

The reference and object waves (disregarding the $[\sin(N\gamma)\sin\gamma]^2$ envelope) can be written as

$$\begin{aligned} R &= R_0\left(\mathrm{e}^{\mathrm{i}(k_1\Gamma_{R1}+\varphi_1)} + \mathrm{e}^{\mathrm{i}(k_2\Gamma_{R2}+\varphi_2)}\right)\,,\\ S &= S_0\left(\mathrm{e}^{\mathrm{i}(k_1\Gamma_{S1}+\varphi_1)} + \mathrm{e}^{\mathrm{i}(k_2\Gamma_{S2}+\varphi_2)}\right)\,, \end{aligned} \tag{9}$$

where $\Gamma_{S(R)i}$ is the object (reference) beam optical path of laser i under angle α_i. As in Sect. 2.1 one obtains from (2) and (6) the resulting intensity of the reconstructed object image

$$\begin{aligned} I_D = \eta_0 I_R\big\{1 + \chi^2 + 2|\chi| \\ \times\cos[2k_1(\Gamma_{S1} - \Gamma_{R1}) - 2k_2(\Gamma_{S2} - \Gamma_{R2})]\big\}\,. \end{aligned} \tag{10}$$

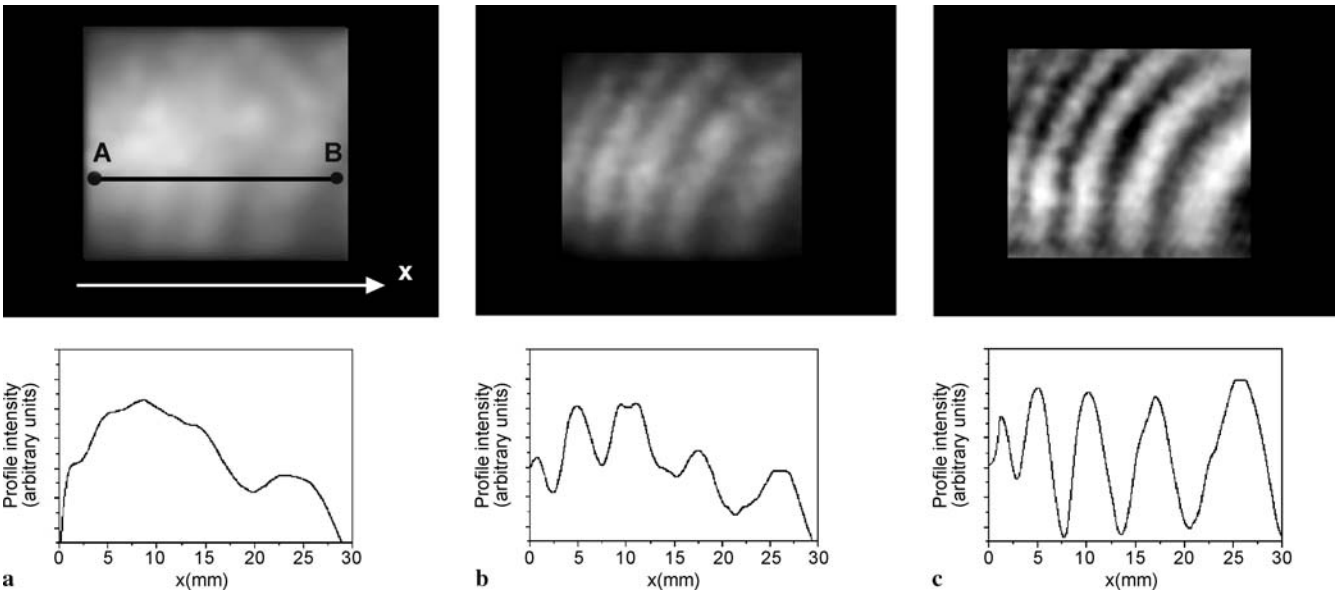

FIGURE 2 Holographic image of a flat bar: (**a**) covered by a single low spatial frequency $[\sin(N\gamma)/\sin\gamma]^2$-fringe; (**b**) covered by high spatial frequency fringes with $\Lambda_S = 0.30$ mm; (**c**) without the low frequency $[\sin(N\gamma)/\sin\gamma]^2$-envelope

From (10) the phase of a point A on a bright fringe is given by

$$k_1\Gamma_{S1A} - k_2\Gamma_{S2A} - k_1\Gamma_{R1} + k_2\Gamma_{R2} = 2q\pi\,, \tag{11}$$

while the phase of a point B on an adjacent bright fringe is

$$k_1\Gamma_{S1B} - k_2\Gamma_{S2B} - k_1\Gamma_{R1} + k_2\Gamma_{R2} = (2q+1)\pi\,, \tag{12}$$

where $q = 1, 2, 3...$ and $\Gamma_{SA(B)}$ is the optical path of the object wave through point A(B). Let us denote gratings 1 and 2 as those recorded by lasers 1 and 2, respectively. Both gratings have slightly different spatial frequencies and are slightly slanted with respect to each other due to the lasers small misalignment. A reference wave of a wavelength λ_1 will interact with both gratings, thus generating two diffracted waves, as mentioned in Sect. 2.1. Due to the misalignment and the lasers detuning, both waves emerge from the crystal with the phase difference ξ [15]. Since ξ does not depend on the surface relief, the influence of the misalignment of the reference beams on the contour interval is negligible. Thus, from (11) and (12) one gets

$$k_1(\Gamma_{S1B} - \Gamma_{S1A}) - k_2(\Gamma_{S2B} - \Gamma_{S2A}) = 2\pi\,. \tag{13}$$

Figure 3 shows the incidence of illuminating beam 1 at angle α on points A and B separated by a distance Δz. If the incidence angle of beam 2 (not shown in this figure) is $\alpha + \Delta\alpha$, the optical path differences between points A and B due to beams originating from lasers 1 and 2 (Fig. 3) are determined to be

$$\begin{aligned}\Gamma_{S1A} - \Gamma_{SB} &= 2\Delta z\cos^2(\alpha/2)\\ \Gamma_{S2A} - \Gamma_{S2B} &= 2\Delta z\cos^2[(\alpha+\Delta\alpha)/2]\,,\end{aligned} \tag{14}$$

where $\Delta\alpha$ is the beam misalignment. For small $\Delta\alpha$, the contour interval can be thus obtained from (13) and (14) after simple algebraic manipulation:

$$\Delta z \cong \left[\frac{2(\lambda_2-\lambda_1)}{\lambda^2}\cos^2\left(\frac{\alpha}{2}\right) - \frac{\Delta\alpha}{\lambda}\sin\alpha\right]^{-1}\,, \tag{15}$$

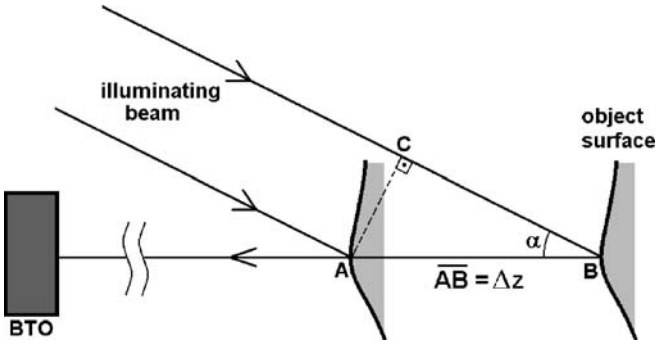

FIGURE 3 Incidence of the illuminating beam onto points A and B distant separated by Δz

where $\lambda^2 = \lambda_1\lambda_2$ and $|\lambda_2 - \lambda_1| \ll \lambda$. Notice that for $\lambda_1 = \lambda_2$ the contour interval reduces to the result obtained for holographic profilometry through the rotation-source method [2, 17]. Thus, the misalignment $\Delta\alpha$ between the beams 1 and 2 in the real-time two-laser method is equivalent to the small tilt angle applied on the illuminating mirror in the two-exposure rotation-source technique. As expected, when the lasers are perfectly aligned, $\Delta z = \Lambda_S/(2\cos^2\alpha/2)$, which is identical to the contour interval obtained elsewhere [4, 7]. Equation (15) is closely related to the dephasing measure ϑ mentioned in Sect. 2.1, showing that laser detuning and beam misalignment produce similar effects. In addition, both $\lambda_2 - \lambda_1$ and $\Delta\alpha$ can be set so as to cancel or mutually enhance their individual effects, since $\Delta\alpha$ can assume both positive and negative values. Hence, the interferogram spatial frequency $1/\Delta z$ can be regarded as a measure of how far from the Bragg regime the wave from laser 1 (2) is diffracted by grating 2 (1).

3 Experimental setup

The two-laser holographic setup is shown in Fig. 4. Both 30-mW diode lasers (Laserline, model LRM-40/650)

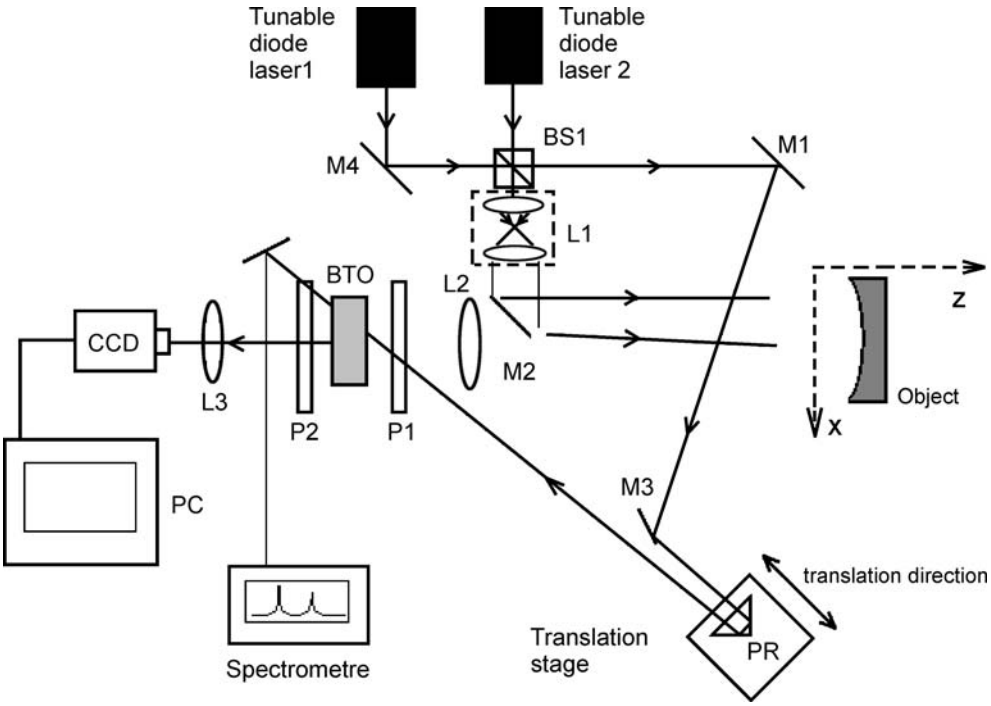

FIGURE 4 Optical setup: M1–M4 – mirrors; L1–L3 – lenses; P1 and P2 – polarizers; BS1 – beam splitter; BTO – $Bi_{12}TiO_{20}$ crystal; CCD; camera; PC; computer

with emissions centered at 670 nm were coupled by the beam splitter BS. Mirror M4 made the propagation of both laser beams collinear after BS. The BTO crystal was placed at the image plane of lens L2, with the CCD camera (Sony SSC-C104, 768 × 494 pixels) focused on the image plane of lens L3 in order to visually display the holographic image. L1 is an afocal telescope which collimates the beam illuminating the object. In order to achieve smaller values of the contour interval Δz without significant loss of the diffraction efficiency, the intersection region of the reference and the object beams inside the crystal was adjusted to be ~ 2 mm, which can be regarded as the effective crystal thickness for Bragg selectivity estimation. In our setup the angle between the recording beams was $2\theta \approx 90°$. The crystal with front face 10×10 mm^2 and thickness 8 mm was cut in the transverse electrooptic configuration [110] and the holographic recording occurred in the pure diffusion regime with a hologram build-up time of ~ 10 s and an acquisition time of ~ 60 s for the four interferograms. The refractive index of the BTO crystal is $n_0 \approx 2.6$ in the red region. By using the anisotropic diffraction properties of the sillenite crystals, polarizer P1 selected the input polarization angle $\varrho L/2$ with respect to the crystal $\langle 001 \rangle$-axis, where ϱ is the crystal rotatory power. This allowed the transmitted object and diffracted waves to be orthogonally polarized at the BTO output [18]. By cutting off the transmitted beam through analyser P2, only the reconstructed object image was observed. For the phase stepping procedure a 90°-prism PR was mounted on a translation stage in order to work as a constant deviation reflector, so the spatial superposition of the interfering beams at the BTO crystal was kept constant as the phase shifts were applied. The other arm of the interferometer containing the transmitted object beam and its holographic reconstruction was used for laser spectrum monitoring. This beam was delivered to a goniometer with a 1200-lines/mm diffraction grating.

As will be seen in the following sections, relatively large synthetic wavelengths compared to the precision of the translation stage (0.001 mm) were used, resulting in a low sensitivity to phase shifting errors of the four stepping procedure.

4 Results and discussion

4.1 *Influence of laser misalignment on the contour interval*

The initial dependence of the contour interval on the misalignment angle $\Delta\alpha$ was analysed. By properly setting this angle, convenient values of Δz were easily obtained without the need of further laser tuning. Hence, setting slight misalignments actually worked as a fine Δz adjustment. Obviously $\Delta\alpha$ or $\lambda_2 - \lambda_1$ cannot be set to indefinitely large values in order to increase the contour sensitivity since a highly out-of-Bragg holographic reconstruction would significantly decrease the hologram diffraction efficiency and spoil the interferogram visibility. For practical purposes, considering our experimental conditions, it was not worthwhile measuring $\Delta\alpha$ since its typically very small values led to relatively large errors. Instead we measured Δz directly by choosing a reference point on the interferogram displayed on the monitor screen and measured the displacement applied to the reference beam as the fringes ran through this point. For p running fringes after a displacement $\Delta\Gamma_R$, the contour interval is given by $\Delta z = \Delta\Gamma_R/p$. Figure 5 shows interferograms of a curved and smooth aluminum surface obtained for $|\lambda_2 - \lambda_1| = 0.2$ nm and $\lambda = 671$ nm, which gives $\Lambda_S = 2.2$ mm. Although the optics of the system was designed and adjusted in order to make the speckle size significantly smaller than the CCD pixel, low-pass FFT filtering was applied in order to reduce speckle noise. In this case lasers 1 and 2 operated in monomode employing a Fabry–Pérot etalon at each

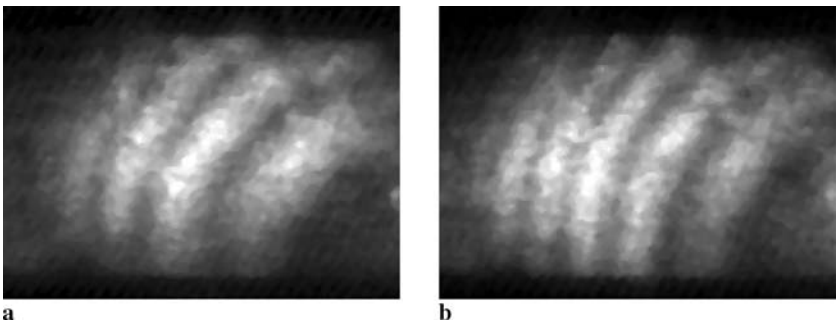

FIGURE 5 Contour interferogram of a curved surface for $\Lambda_S = 2.2$ mm and (**a**) $\Delta\alpha \approx 1.6 \times 10^{-4}$ rad and $\Delta z \cong 1.7$ mm; (**b**) $\Delta\alpha \approx -5 \times 10^{-5}$ rad and $\Delta z \cong 1.4$ mm

laser output. From the interferogram shown in Fig. 5a the contour interval was measured to be $\Delta z \cong 1.7$ mm and the misalignment was estimated to be $\Delta\alpha \approx 1.6 \times 10^{-4}$ rad using the methods of (15). In Fig. 5b, $\Delta z \cong 1.4$ mm and $\Delta\alpha \approx -5 \times 10^{-5}$ rad. In both cases, $\alpha \approx 0.5$ rad. The rather poor visibility of the interferograms in both figures is due to the fact that the diffraction efficiency in the out-of-Bragg holographic reconstruction was estimated to be $\sim 20\%$ of that in the Bragg regime, i.e. $\chi^2 \approx 0.2$ in (6), giving $V \approx 0.37$. The data was obtained from the experimental parameters with the help of the expressions shown at the end of Sect. 2.1.

4.2 *Determining the slope of an integrated circuit*

We performed the profilometric measurement of an 15×8 mm^2-integrated circuit (IC). This is a subject of great interest in the study of chip packaging interaction in order to reduce stresses and deformation and to improve packaging reliability [19]. In order to allow an easier fringe visualization, the IC was slightly tilted with respect to the front face of the BTO crystal. The $\cos^2$-interferogram shown in Fig. 6a was obtained by dividing the original interferogram by the holographic image taken with only one multimode laser, as described in Sect. 2.2. Figures 6b and c show the phase map and the 3-D plot of the integrated circuit for $\Delta z = 0.35$ mm. From 5a and b and from the lower part of Fig. 6c (with the z- versus x-coordinate for $y = 2$ mm) the IC flatness was estimated to be ≈ 90 μm.

4.3 *Measurement of small surface irregularities*

The measurement of a slightly curved metallic plate was carried out in order to evaluate the capacity of the method in evaluating small superficial structures and details. The plate was covered by a opaque tape in such a way to introduce some small relief irregularities. By tuning the lasers and adjusting the optical setup, the contour interval was obtained to be $\Delta z = 0.15$ mm. Figure 7a shows the interferogram of the first frame, while Fig. 7b shows the corresponding phase map obtained through (7). By unwrapping the phase through the branch-cut method one obtains the 3-D reconstruction of the plate shown in Fig. 7c. The three-dimensional plot of the studied surface is in very good agreement with the actual object shape. Through our optical profilometry method the height of the central elevation shown in Fig. 7c was measured to be 140 μm, which is in accordance with the value of ~ 130 μm obtained with a mechanical height gauge. The discrepancy between the values can be attributed to the fact that the mechanical contact of the gauge with the soft surface produced small deformations during the measurement.

5 Conclusion

Holographic profilometry employing two tunable diode lasers and a BTO crystal was performed, and the reliefs of low-derivative surfaces were measured. The theoretical description of the holographic recording and readout was developed for two multimode diode lasers, showing that

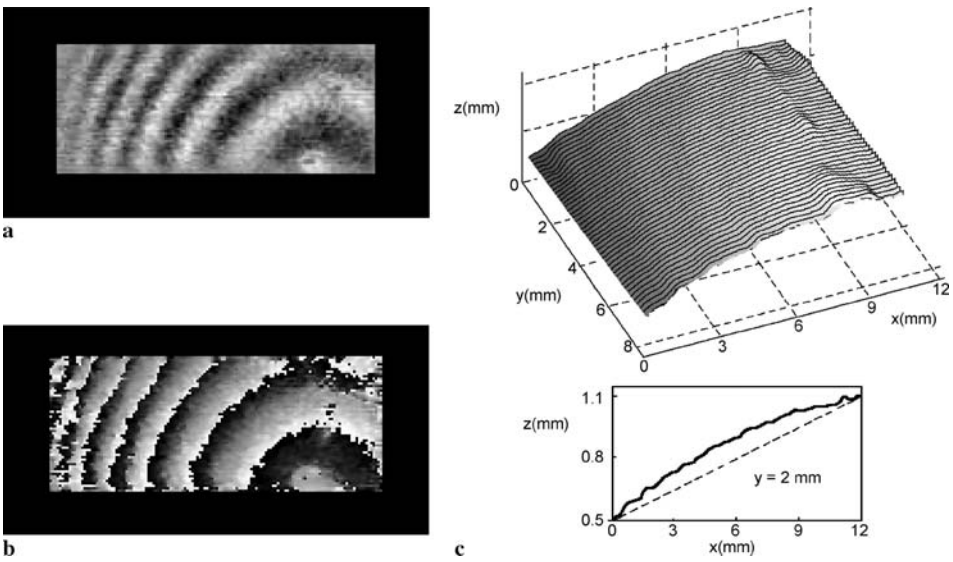

FIGURE 6 Two-diode laser profilometry of an IC surface: (**a**) interferogram for $\Delta z = 0.35$ mm; (**b**) phase map; (**c**) 3-D reconstruction

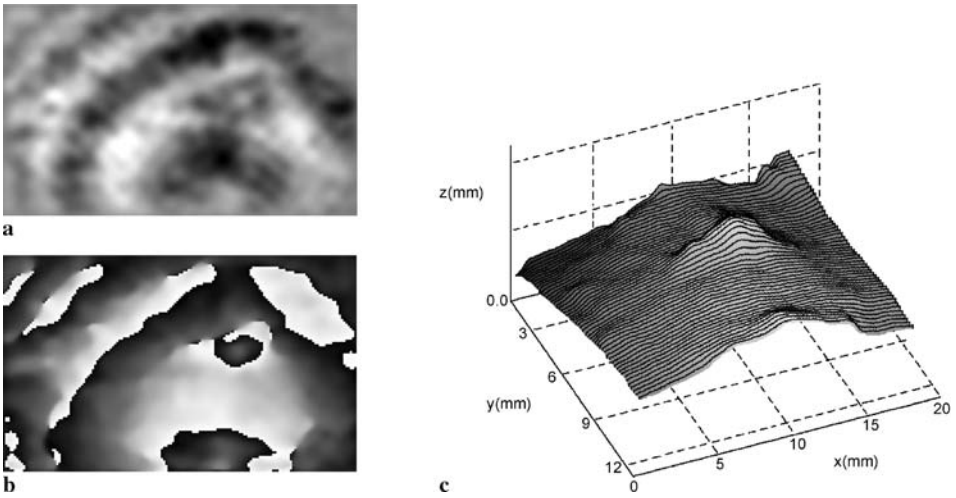

FIGURE 7 Shape measurement of an irregular surface for $\Delta z = 0.15$ mm: (**a**) interferogram; (**b**) phase map; (**c**) 3-D reconstruction

the resulting real-time single-exposure high spatial frequency contour fringes are modulated by a low spatial frequency envelope due to the multi-wavelength emission of each laser. The dependence of the contour interval on the lasers wavelengths and their misalignment was also studied, describing the relation between the interferogram spatial frequency and the deviation from the Bragg regime. The results established the conditions through which the lasers can be tuned and aligned in order to provide small contour intervals without significant loss of interferogram visibility.

Two procedures for eliminating the low spatial frequency envelope were described and employed, significantly enhancing the interferogram visibility for visual inspection and allowing quantitative evaluation through the four stepping method. The profilometry technique presented in this work points out promising potentialities for nondestructive testing, providing very precise and fast measurements as well as accurate qualitative analysis. The anisotropic diffraction properties, high optical quality and high resolution of BTO crystals enable them to obtain very small contour intervals, resulting in lower measurement noise. This was found to circumvent the intrinsic low visibility of interferograms and aid in visualization.

ACKNOWLEDGEMENTS We thank Prof. E.A. Affonso from Centro Federal de Educação Tecnológica and A.O. Preto from Faculdade de Tecnologia de São Paulo for fruitful discussions.

REFERENCES

1 G. Gülker, O. Haack, K.D. Hinsch, C. Hölscher, J. Kuls, W. Platen, Appl. Opt. **31**, 4519 (1992)
2 G. Pedrini, P. Fröning, H.J. Tiziani, F.M. Santoyo, Opt. Commun. **164**, 257 (1999)
3 M.R.R. Gesualdi, E. Gonçalves, R. de Souza, F.F. Palácios, M. Muramatsu, J. Valin, A. Marcano, J.L. Paz, Proc. SPIE **5622**, 1422 (1997)
4 E.A. Barbosa, A.A.V. Filho, M.R.R. Gesualdi, B.G. Curcio, M. Muramatsu, D. Soga, J. Opt. Soc. Am. A **22**, 2872 (2005)
5 E.A. Barbosa, M.R. Gesualdi, M. Muramatsu, Y. Sheng, S. Zhuang, Y. Zhang, Proc. SPIE **6027**, 522 (2005)
6 E.A. Barbosa, Appl. Phys. B **80**, 345 (2005)
7 M. Muramatsu, E.A. Barbosa, E.A. Lima, M.R.R. Gesualdi, P. Slangen, C. Cerruti, Proc. SPIE **6341**, 210 (2006)
8 E.A. Barbosa, A.C. Lino, accepted for publication in Appl. Opt. (2007)
9 E. Hack, B. Frei, R. Kästle, U. Sennhauser, Appl. Opt. **37**, 2591 (1998)
10 T. Maack, G. Notni, W. Schreiber, Opt. Commun. **115**, 576 (1995)
11 K. Creath, *Phase Measurement Techniques: Progress in Optics XXVI* (Elsevier Science Publishers, Amsterdam, 1988)
12 J.M. Huntley, Appl. Opt. **28**, 3268 (1989)
13 B. Gutmann, H. Weber, Appl. Opt. **38**, 5577 (1999)
14 P. Günter, J.P. Huignard (eds.), *Photorefractive Materials and Their Applications II*, Topics in Appl. Phys. Vol. 62 (Springer, Berlin Heidelberg, 1989)
15 H. Kogelnik, Bell Syst. Tech. J. **48**, 2909 (1969)
16 K. Creath, J. Schmit, Opt. Lasers Eng. **24**, 365 (1996)
17 I. Yamaguchi, S. Ohta, J.I. Kato, Opt. Lasers Eng. **36**, 417 (2001)
18 A.A. Kamshilin, M.P. Petrov, Opt. Commun. **53**, 23 (1985)
19 G. Wang, C. Merrill, J.-H. Zhao, S.K. Groothuis, P.S. Ho, IEEE Trans. Dev. Mater. Reliab. **3**, 119 (2003)